Research Article

A Simplified Model for Propeller Thrust in Oblique Flow

Christian Patience[1], Meyer Nahon[1]

1. Department of Mechanical Engineering, McGill University, Canada

New aircraft architectures are being proposed for unmanned aerial vehicles and air taxis, which include tiltable motor and propellers. These propulsive units operate with a propeller axis at an angle oblique to the flight direction, and thus it is important to understand and model how thrust is produced by a propeller operating under these conditions. Propellers in oblique flow have been modeled using Blade Element Momentum Theory coupled to an inflow model, and the Vortex Lattice Method. In the present work, we develop a much simpler approach that neglects the crossflow component of the incoming air velocity. An advance ratio is developed based on the parallel inflow component, and is coupled to existing propeller data collected in axial flow conditions. The proposed model is evaluated using existing experimental data collected under oblique flow conditions, and is predicts thrust to within $5\,\%$ of experimental values for most conditions. The greatest discrepancy between the model and experiments occurs in the pure crossflow case, which is of lesser importance in the application to unmanned aerial vehicles and air taxis.

Correspondence: papers@team.qeios.com — Qeios will forward to the authors

Nomenclature

ν = fluid freestream velocity

T = propeller thrust [N]

ρ = density [kg m^{-3}]

n = propeller rotational velocity [rev s^{-1}]

ω = propeller rotational velocity [rad s^{-1}]

D = propeller diameter [m]

k_T = generic static thrust coefficient

C_{T_0} = static coefficient of thrust

C_T = coefficient of thrust

J = advance ratio

 doi.org/10.32388/WG08LV

ς = oblique angle [°]

$f(\nu, \varsigma, n)$ = flow condition at (ν, ς, n)

Subscripts

$\|$ = parallel to propeller spin axis

$\perp$ = perpendicular to propeller spin axis

exp = experimental data

max = maximum

I. Introduction

Unmanned aerial vehicles (UAVs) are increasingly being employed in a wide range of applications, including wildfire surveillance, crop or forest fire monitoring, search and rescue, and transport of medical supplies. More recently, UAVs have been proposed as a form of urban air taxi[1]. Most of these applications use aircraft that can be classified as either multi-rotor vertical takeoff and landing, or fixed-wing. The former are generally more maneuverable, whereas the latter excel in longer-distance transit. Recently, an increasing number of hybrid UAVs have been proposed to combine the advantages of both architectures: multi-rotor vertical takeoff with high maneuverability, and fixed-wing flight for longer distances. These take on many different forms, including tilt-rotor, tilt-wing and tailsitters[2].

Many of these new architectures have relatively small wing surface area, and require the rotors to supplement the wing lift. Thus, the rotors may not be oriented purely horizontally but are tilted forward and upward (Fig. 1). In these configurations, the rotors operate in oblique flow, where the axis of the rotors and the direction of flight are not parallel. Moreover, rotors often operate in oblique flow for agile UAVs[3], which specialize in extreme aerobatic maneuvers such as for obstacle avoidance.

Figure 1. Joby Aviation tilt-rotor[4]

Thrust modeling and prediction of propellers operating in oblique flow is important in the design and control of UAVs that routinely operate under these conditions. For example, accurately predicting thrust for a particular flight condition and rotor speed ensures the motor commands will produce the thrust appropriate for the maneuver. Additionally, the model must be computationally simple for it to be solved at a high update rate in real time when used in a controller.

Most literature on propeller-driven UAVs implement very simple thrust modeling, i.e. $T = k_T \omega^2$, with the thrust coefficient k_T being determined experimentally or from a Blade Element Momentum Theory (BEMT) analysis. With a constant thrust coefficient, k_T, this corresponds to static conditions. More sophisticated models account the loss of thrust loss due to forward speed by varying the thrust coefficient with the advance ratio $J = \nu / nD$. This model assumes that the rotors operate in axial flow, where the flow direction is aligned with the propeller axis. The University of Illinois at Urbana-Champaign[5] maintains a comprehensive database of a wide range of UAV propeller thrust characteristics generated from wind tunnel experiments. For propellers not in this database, BEMT can instead estimate thrust vs. advance ratio characteristics with less precision.

The characterization and modeling of UAV propellers in oblique flow conditions has been studied for conventional propeller-driven aircraft. Specifically,[6][7] investigated the influence of small-to moderate angle of attack or sideslip angle on the generation of thrust. These works are mainly limited to angles less than about 15° between the propeller axis and the inflow angle. Oblique flow into a rotor has also been studied for helicopters in forward flight[8]. Glauert[9] treated a rotor disc in forward flight as analogous to a circular wing, and applied lifting line theory to deduce a model for the inflow through the disc. Many subsequent analyses

doi.org/10.32388/WG08LV

build on this to propose alternative inflow models, and a survey of these models was assembled by [10]. An inflow model can be coupled to a BEMT analysis of the rotor to predict the thrust, other forces perpendicular to the thrust axis, and moments.

The increasing global interest in hybrid and agile UAVs has motivated research in developing models for the full set of forces and moments generated by a UAV propeller in oblique flow. Analogous to the work on helicopter rotors, a BEMT analysis has been coupled to an inflow model to predict the full suite of forces and moments produced by a UAV propeller in oblique flow[11]. Additionally, a Vortex Lattice Method (VLM) was applied to predict these forces and moments under oblique flow conditions[12]. In parallel to the modeling approaches, wind tunnel experiments measure the forces and moments directly in various oblique flow conditions. Researchers at KUL[12] performed a range of tests on a Graupner Elektro 9x5 propeller at wind tunnel speeds up to 6 m s^{-1}, and oblique angles from zero to 90°. More recently, researchers at ETH[13] performed wind tunnel experiments on nineteen UAV propellers, at speeds up to 18 m s^{-1} and oblique angles from zero to 90°.

The models proposed in [11][12][13] are complex to develop and to implement. Moreover, models based on BEMT[11] or VLM[12] are unlikely to be solved in real-time. The approximate models presented in [13] acknowledge the need for fast models, and ideally ones that could build on the available data in [5]. The purpose of the current work is to present a simplified model for the thrust produced by UAV propellers operating under general oblique conditions. Here we develop a simpler approach that neglects the crossflow component of the incoming air velocity. The model relies on propeller characterization data collected in pure axial conditions, coupled to an assumption that the flow perpendicular to the thrust axis can be neglected. The proposed model predicts thrust to within $5\,\%$ of experimental measurements for most conditions.

II. Generation of Thrust in Axial Flow

A propeller generates thrust by changing the momentum of the air passing through it as the blades rotate, i.e., $T = 2\dot{m}w$, where $\dot{m} = \rho(\nu + w)A$ is the mass flow rate of air through the rotor of area A, ν is the freestream velocity and w is the speed increase of the air at the propeller. Momentum theory predicts that far downstream of the propeller, the speed increase of the air is twice what it was at the propeller[8]. In reaction, the air exerts a force and a torque along the rotational axis of the propeller. If the freestream flow has some positive velocity, the mass flow rate through the propeller is increased, but the speed increase through the propeller, w, is reduced, leading to a net reduction in the momentum imparted to the air, and a lower thrust than if the flow had no inflow velocity.

The thrust produced by a propeller can be characterized in non-dimensional form using[5]:

$$C_T = \frac{T}{\rho n^2 D^4} \tag{1}$$

where C_T varies with J. The advance ratio represents a ratio of the freestream velocity of the fluid to the tip velocity of the propeller:

$$J = \frac{\nu}{nD} \tag{2}$$

The relationship between C_T and J captures the loss of thrust with an increasing fluid velocity. Experiments conducted by [5] (and hosted on the UIUC propeller data website) demonstrate this effect (Fig. 2). Fig. 2a maintains $\nu = 0$ m s^{-1}, and varies the propeller rotational velocity to characterize the *static* thrust coefficient C_{T_0}, while Fig. 2b shows the decrease in C_T as J is increased. The flow condition $\nu = 0$ m s^{-1} provides the *static* thrust coefficient, C_{T_0}, and is relatively constant with n (Fig. 2a). On the other hand, the non-static thrust coefficient C_T given by $\nu > 0$ m s^{-1} decreases as J increases (Fig. 2b).

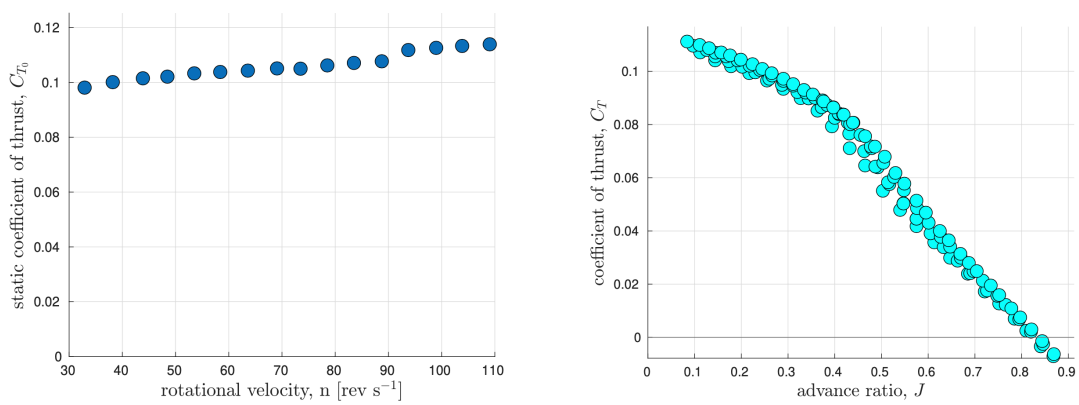

(a) Static coefficient of thrust, C_{T_0}, versus rotational velocity, n **(b) Coefficient of thrust, C_T, versus advance ratio, J**

Figure 2. Coefficient of thrust, C_T, versus advance ratio, JWind tunnel experiments performed by [5] for propeller APC Thin Electric 10x7

This relationship holds for a multitude of other propellers taken from [5] (Fig. 3). The common trend among C_{T_0} is that it remains stable over a wide range of n (Fig. 3a), whereas C_T decreases with increasing J even beyond $C_T < 0$ (Fig. 3b). A negative C_T indicates that in the current flow conditions and propeller rotational velocity, the thrust generated is directed rearward. Common implementations of the effects of advance ratio ignore these flow conditions and saturate the corresponding thrust to a minimum bound of zero.

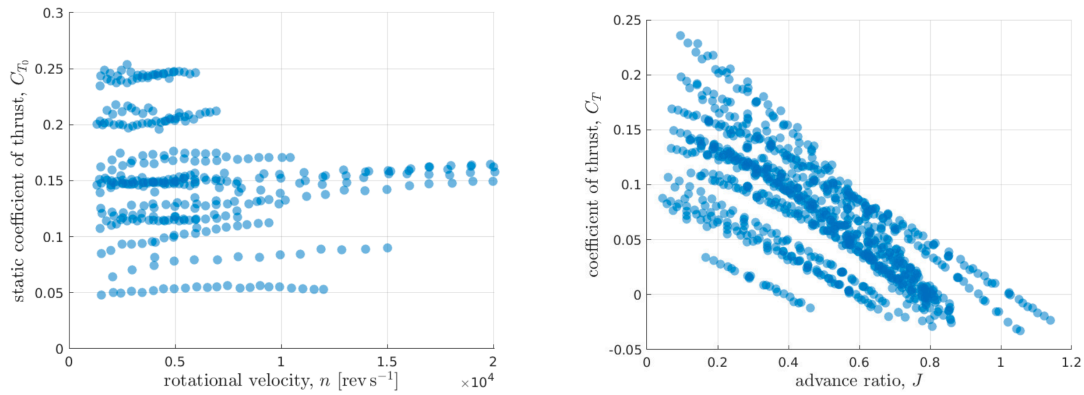

(a) Static coefficient of thrust, C_{T_0}, versus rotational velocity, n **(b) Coefficient of thrust, C_T, versus advance ratio, J**

Figure 3. Coefficient of thrust, C_T, versus advance ratio, JWind tunnel experiments performed by [5]. Chosen 12 propellers arbitrarily from their dataset.

Models based on the advance ratio, $C_T(J)$ (Fig. 3), 2), are not always feasible because they require experimental tests in a wind tunnel. An alternative is to use BEMT for axial flow to generate these $C_T(J)$ curves[14]. This approach is computationally straightforward but requires detailed knowledge of the blade geometry in order to produce good results.

While $C_T(J)$ for axial flow can be generated experimentally and computationally, its application remains limited to situations where the incoming flow is parallel to the thrust vector of the propellers. In the case of quadrotors, it is common practice to linearize around hovering conditions, in which case the thrust can be based on Fig. 3a. Moreover, quadrotor motion generally follows the direction of thrust of their propellers such as during takeoff, landing, and maneuvers that require high thrust. In these cases thrust is reasonably characterized by Fig. 3b. These assumptions are less justified for tilt-rotor aircraft, which may be travelling forward with the propellers pointed at a large angle relative to the direction of motion.

III. Generation of Thrust in Pure Crossflow

Pure crossflow is the condition in which the air velocity is purely perpendicular to the propeller rotational axis. In this condition, the momentum of the air in the direction along the axis of the propeller is initially zero, and the propeller then imparts some momentum to the air in that direction to generate thrust. This is the case in static flow as well, where the ambient flow has zero incoming momentum. Assuming the thrust is only due to the momentum change along the propeller axis, the thrust behaviour of a propeller in pure crossflow should be similar to the same propeller in static conditions. Experiments conducted by [12] allow us to make this comparison (Fig. 4), and demonstrate that propeller thrust is largely unaffected by pure crossflow; the propeller

is able to produce similar amounts of thrust in spite of the strong crossflow. This suggests that the flow along the axis of the propeller is largely unaffected by the by the flow perpendicular to that axis, and motivates a model that considers only the *axial* inflow velocity to be relevant in the generation of thrust.

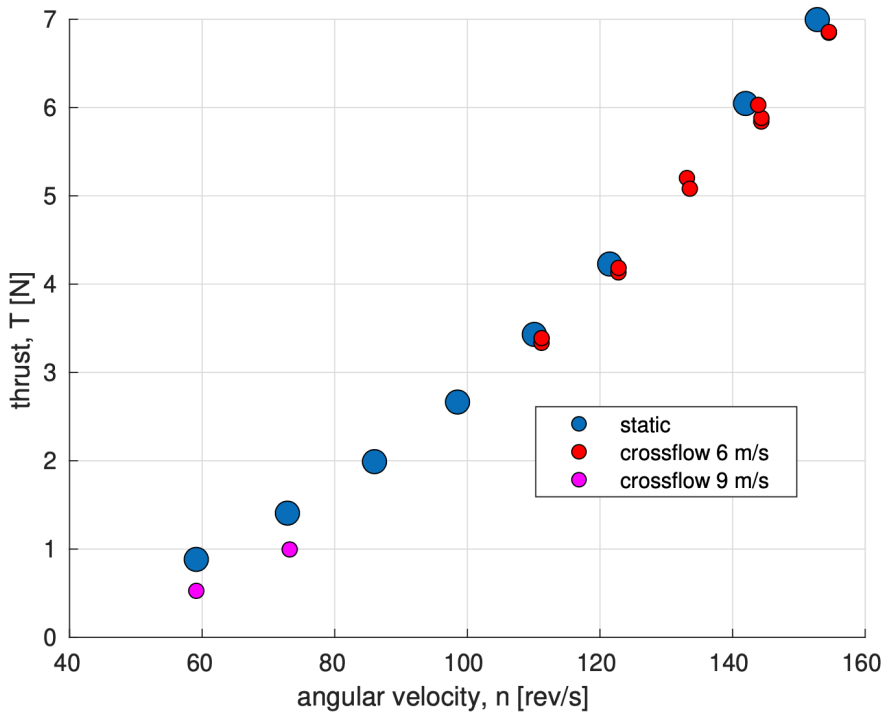

Figure 4. Thrust, T, versus rotational velocity, n, in static conditions (blue) and in crossflow conditions at $\nu = 6$ m s^{-1} (red) and $\nu = 9$ m s^{-1} (magenta) for propeller Graupner Elektro 9x5.

IV. Modeling Thrust in Oblique Flow

As noted earlier, BEMT has been used to model the generation of forces and moments generated by a propeller in oblique flow, coupled with an inflow model for the airflow profile at entry to the propeller[11]. Computational fluid dynamics can also be used to predict these forces and moments, such as [12]'s VLM, which yielded reasonable results. These methods can be computationally expensive, making them inappropriate for use where real-time execution or quick turnaround is needed.

Momentum theory can be used to analyze oblique flow through a rotor, and considers thrust to be produced by the change of velocity of a mass flow rate of air through the propeller. In the oblique flow analysis applied to a helicopter in forward flight[8], the thrust produced is again found to be $T = 2\dot{m}w$, but now, $\dot{m} = \rho A\sqrt{(\nu\cos\alpha)^2 + (\nu\sin\alpha + w)^2}$, while the velocity increment through the propeller is found to be

doi.org/10.32388/WG08LV

$$w = \frac{T/(2\rho A)}{\sqrt{(\nu\cos\alpha)^2 + (\nu\sin\alpha + w)^2}} \tag{3}$$

The model is based on the assumption that the plot of C_T vs J obtained in pure axial flow applies equally well to the axial flow component of the air velocity in oblique flow; that the crossflow air velocity does not affect the production of thrust. In oblique flow conditions, the ambient air velocity, ν, is partitioned into components along the propeller thrust, $\nu_\parallel$, axis and perpendicular to it, $\nu_\perp$ (Fig. 5). The parallel velocity component, $\nu_\parallel$, is the projection of ν onto the direction T, and, by itself, would represent the axial flow condition:

$$\nu_\parallel = \nu\cos\varsigma \tag{4}$$

The perpendicular velocity component is the component of ν that is in pure crossflow to the propeller, and, by itself, represents the crossflow condition. According to our baseline assumption — that crossflow does not affect the thrust — $\nu_\perp$ does not contribute to a loss of thrust due to non-zero J. This leaves just the parallel component, $\nu_\parallel$, which is consistent with the axial flow condition, so that eq. 2 remains valid. We therefore calculate the advance ratio calculated with $\nu_\parallel$ as $J_\parallel$, and it is given by:

$$J_\parallel = \frac{\nu_\parallel}{nD} \tag{5}$$

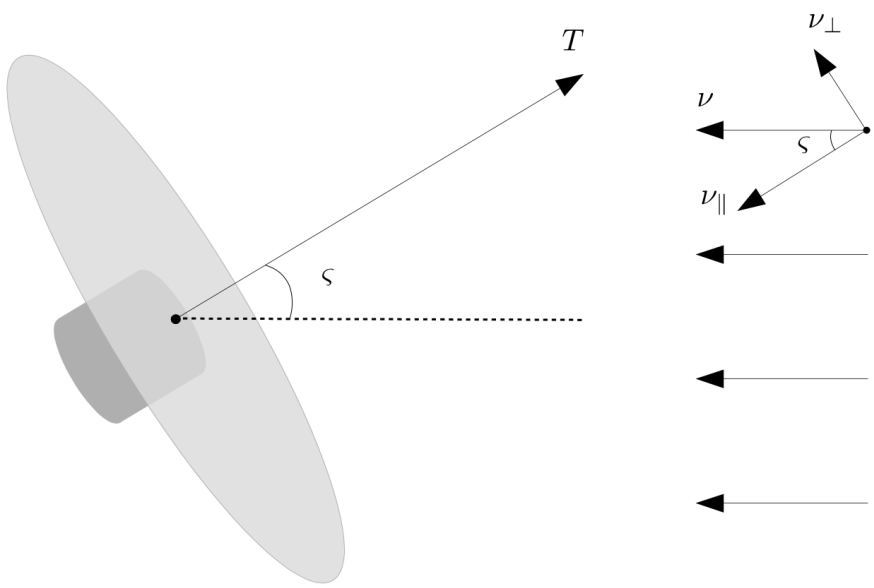

Figure 5. Propeller in oblique flow

The subsequent step is finding a relationship between the coefficient of thrust in oblique flow and $J_\parallel$. To facilitate this, axial flow and static flow experiments are considered to be special cases of oblique flow. Axial flow is equivalent to oblique flow at $\varsigma = 0°$, and static flow at $\varsigma = 90°$ (with $J = 0$) given the crossflow

doi.org/10.32388/WG08LV

assumption. Thus Fig. 2a and Fig. 2b are merged together and a second order polynomial, $C_T(J)$, is fit to all the data (Fig. 6). The final step is to calculate C_T by inputting $J_{\parallel}$ in the $C_T(J)$ polynomial.

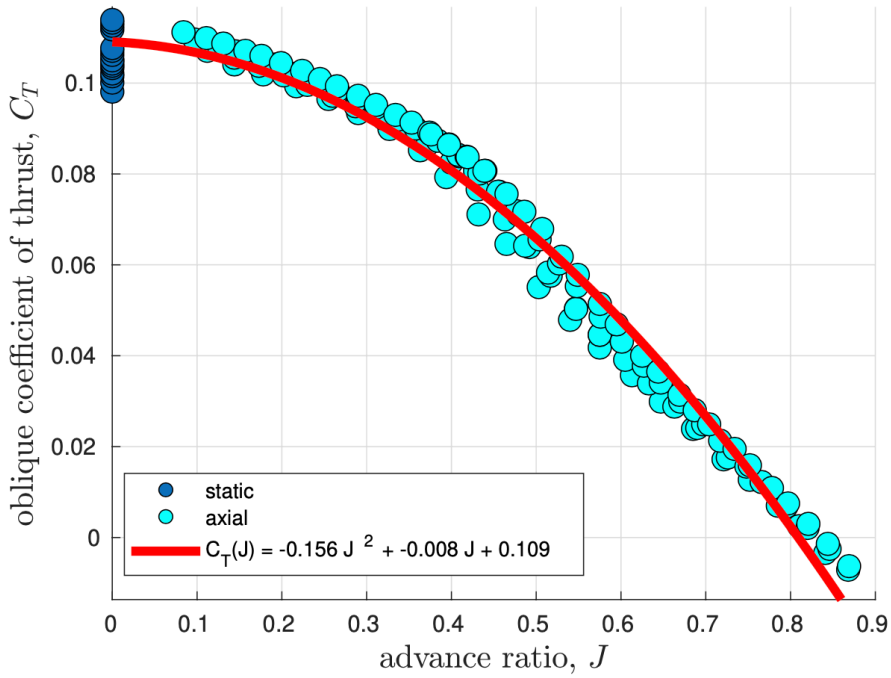

Figure 6. Merged static (cyan) and axial (blue) experimental data from wind tunnel experiments performed by [5] for propeller APC Thin Electric 10x7. Fitted a second order polynomial, $C_T(J)$ (red), to the static and axial data.

V. Model Validation

Two independent datasets are used to validate our proposed thrust model: the KUL experiments[12] and the ETH experiments[13]. In each case, a total of six propeller forces and moments were measured at a range of oblique angles in a wind tunnel.

A. Graupner Elektro 9x5 Propeller Validation

The first validation was performed using force and moment data collected by [12] for the Graupner Elektro 9x5 propeller at a freestream velocity of 6 and 9 m s^{-1} at oblique angles 0°, 30°, 60°, and 90°. Their results from BEMT and VLM models were plotted alongside the experimental data only for $\nu = 6$ m s^{-1} (Fig. 7).

We obtain our $C_T(J)$ polynomial by fitting to their experimental axial ($\varsigma = 0^\circ$, Fig. 7 top left) and static ($\nu = 0$ m s^{-1}) data, resulting in a fitted polynomial of $C_T(J) = -0.154\,J^2 - 0.040\,J + 0.084$. The oblique

doi.org/10.32388/WG08LV

advance ratio, $J_{\parallel}$, is calculated for each flow condition $f(\nu, \varsigma, n)$ with eq. 5. Following this, the $C_T(J)$ polynomial is evaluated at $J_{\parallel}$, and eq. 1 is then used to calculate thrust (Fig. 7, red).

The model's error is the average difference between the experimental thrust, T_{exp}, and the predicted thrust, T, at each n:

$$e_T = \frac{|T_{exp} - T|}{T_{max}} \tag{6}$$

The difference is normalized with respect to the maximum thrust, T_{max}, which is evaluated at the maximum experimental rotational velocity in static conditions (Table 1). The mean error for the flow conditions at which $C_T(J)$ was partially fitted, $f(\nu = 6, \varsigma = 0, n)$, is $\bar{e}_T|_{\varsigma=0^\circ} = 2.3\,\%$. The mean error for the oblique angles remains similarly low, with $\bar{e}_T|_{\varsigma=30^\circ} = 3.8\,\%$, $\bar{e}_T|_{\varsigma=60^\circ} = 2.6\,\%$, $\bar{e}_T|_{\varsigma=90^\circ} = 2.1\,\%$. For each oblique angle, the error is highest at maximum n and, by extension, a low $J_{\parallel}$, with the highest being $e_{T,max} = 11\,\%$ at $\varsigma = 30^\circ$ and $n = 150$ rev s^{-1}. The model tends to underestimate T at high n, whereas the BEMT and VLM models overestimate T. The low error at $\varsigma = 90^\circ$ is consistent with the comparison between static conditions to crossflow (Fig. 4).

These results demonstrate the model's effectiveness in estimating thrust in oblique flow, but the flow conditions were limited to $\nu = 6$ m s^{-1}. Overall, these test conditions had a maximum advance ratio of $J_{max} = 0.44$, occurring at $f(\nu = 6, \varsigma = 0, n = 60)$. For this propeller, C_T remains positive until $J = 0.62$, and so the experimental data spans about $70\,\%$ of the possible J with $C_T > 0$. The subsequent validation includes more diverse flow conditions with a larger advance ratio, and further validates the model.

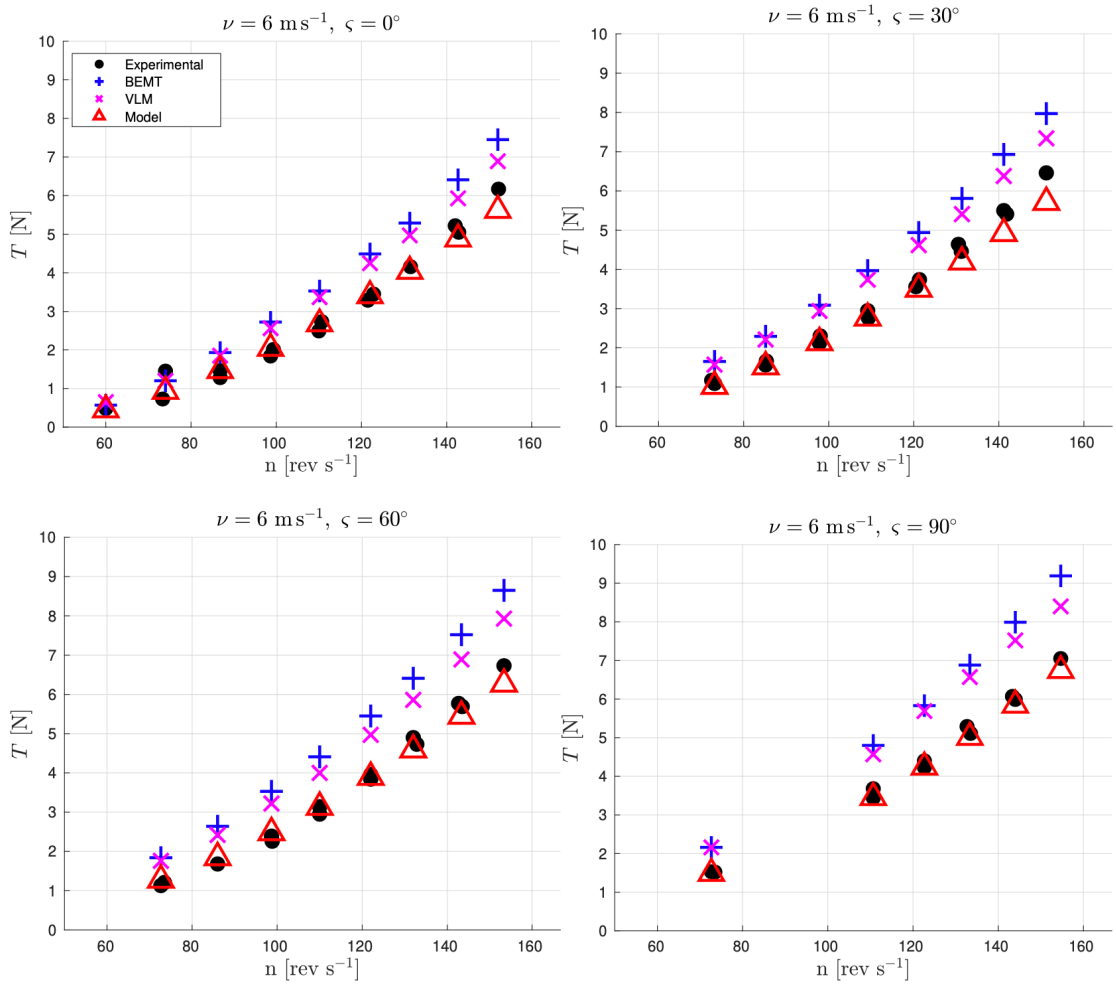

Figure 7. Thrust along the rotational axis of propeller Graupner Elektro 9x5 in a freestream velocity of $\nu = 6$ m s^{-1} at various oblique angles ς. Experimental (black), BEMT (blue) and VLM (magenta) data from [12], are compared to our model (red). The C_T versus J polynomial fitted to the model is $C_T = -0.154\,J^2 - 0.040\,J + 0.084$.

B. APC Propellers Validation

The second validation is performed against four APC propellers whose thrust in oblique flow was measured by [13] in wind tunnel tests. They controlled the freestream velocity, angle of the propeller oblique to the wind, and propeller rotational velocity. The freestream velocity was held constant at $\nu = 10.5$, 16.3, and 6.4 m s^{-1} while slowly varying the oblique angle ς at 0.2° s^{-1} and simultaneously changing the propeller rotational velocity sinusoidally at 0.017 Hz (Fig. 8). The variations were slow enough to allow the quasisteady flow assumption to hold while inducing negligible torque from gyroscopic precession.

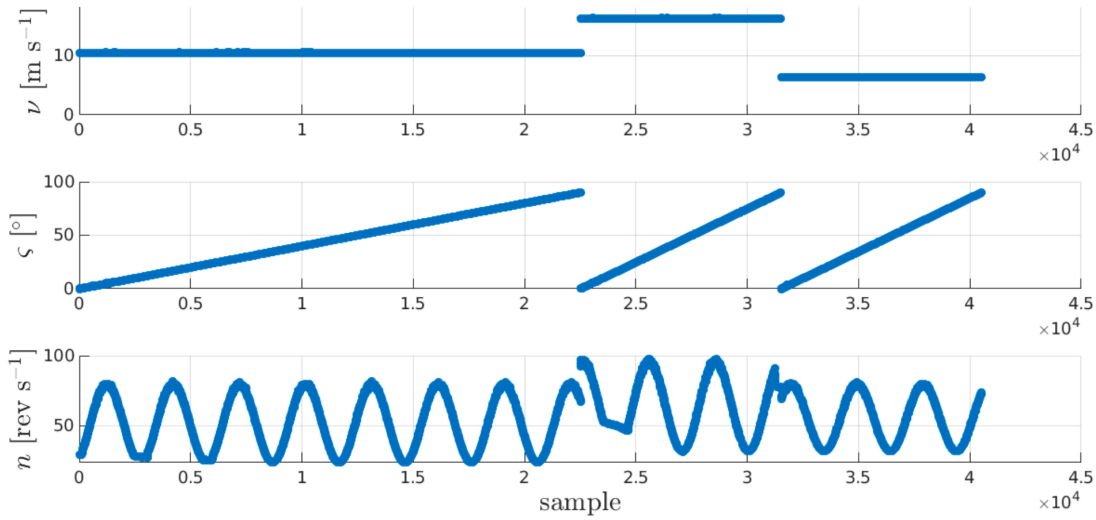

Figure 8. Oblique flow experiment in wind tunnel conducted by [13] for propeller APC Thin Electric 10x7. Top figure plots the freestream velocity, middle plots the oblique angle, and bottom plots the propeller rotational velocity.

In this validation, we obtain the $C_T(J)$ polynomial by fitting to the static and axial data collected by [5], resulting in a fitted polynomial of $C_T(J) = -0.156\,J^2 - 0.008\,J + 0.109$. The oblique advance ratio is calculated from the experimental flow conditions in [13]. The $C_T(J)$ polynomial is then evaluated at this $J_{\parallel}$, and the thrust is once again calculated with eq. 1. Thus, $C_T(J)$ is fitted to [5]'s axial dataset and validated with [13]'s oblique dataset (Fig. 9). The lower subfigure plots the thrust percent error, e_T, between the experimental data and the model at each sample with eq. 6. The maximum thrust is calculated with eq. 1 assuming static conditions and operating at the maximum experimental rotational velocity (Table 1). The average percent error is $\bar{e}_T = 5.1\,\%$.

The error plot indicates that the error is highest for oblique angles approaching 90°, and at high values of ν. By contrast, at relatively low speeds, the Graupner propeller had low error in pure crossflow ($\varsigma = 90°$).

The average error noted above includes flow conditions with negative thrust and high oblique angles which are rarely encountered, and only during transient maneuvers. When evaluated separately for these states, the average percent error increases to $\bar{e}_T = 8.1\,\%$. In steady flight with $T \geq 0$ and $\varsigma \lesssim 75°$, the error drops to $\bar{e}_T = 4.5\,\%$. This is only slightly higher than the error for the Graupner 9x5 propeller despite the polynomial being fitted and validated on data from different sources.

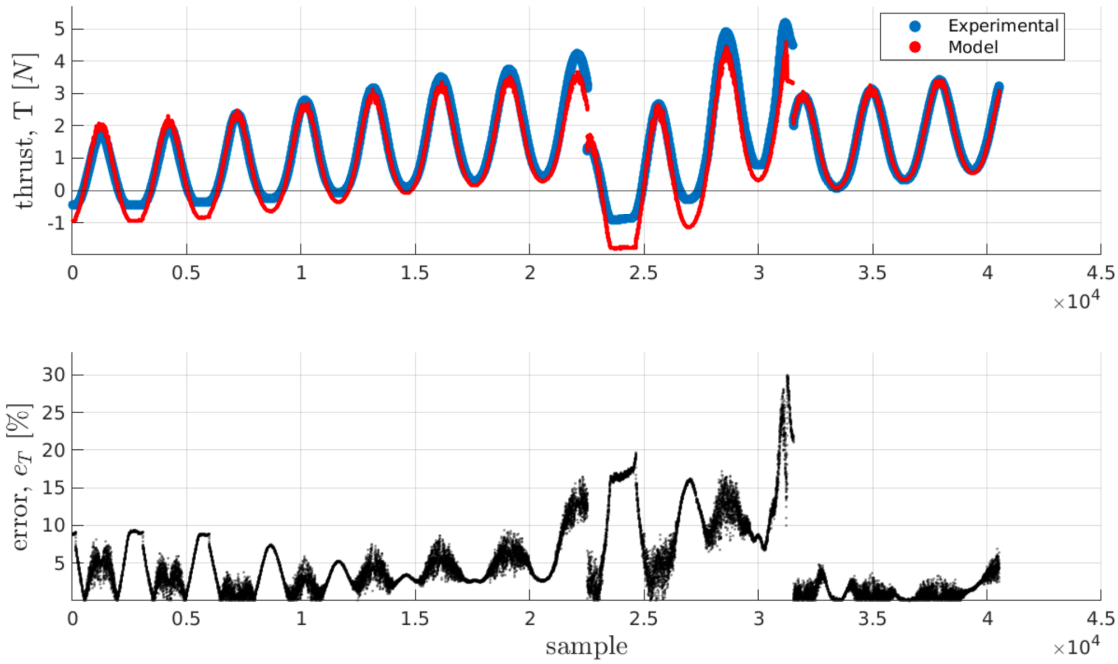

Figure 9. Experimental thrust (top, blue) from oblique flow experiment in wind tunnel conducted by [13] for propeller APC Thin Electric 10x7. Modeled thrust (top, red) at each sample. Bottom figure plots the percent error between the experimental and the modeled data.

Propeller	n_{max} [rev s^{-1}]	T_{max} [N]
APC Thin Electric 8x6	98	2.3
APC Thin Electric 8x8	98	2.6
APC Thin Electric 10x7	98	5.4
APC Slow Flyer 10x4.7	82	4.5
Graupner Elektro 9x5	155	7.1

Table 1. Maximum propeller rotational velocity used in experiments, and corresponding maximum thrust under static conditions.

Analogous results are shown in the Appendix for three other APC propellers: the Thin Electric 8x6, the Thin

Electric 8x8 and the Slow Flyer 10x4.7. In all cases, the results are qualitatively similar to those for the Thin Electric 10x7 discussed here.

VI. Conclusion

Tilt-wing aircraft fly primarily in oblique flow wind conditions. Presently, computational models such as BEMT and VLM are the most common approaches to estiamting thrust under these conditions. Their drawback is their computational copmlexity, which renders them unfit for live implementation in the control loop. Here, we presented a simplified model for the generation of thrust under oblique inflow conditions. The model neglects the cross-flow component of inflow to calculate a propeller advance ratio. This is then used in conjunction with data collected under axial flow conditions to predict the thrust in oblique flow conditions. When evaluated against experiments performed in oblique flow conditions, the model produces thrust predictions within $5\,\%$ of experimental values for most conditions. The main limitation is that the model errors can be significantly higher as oblique angles approach 90°. However, this pure cross-flow case is less important to tilt-wing aircraft, whose rotors operate primarily in oblique flow. This simple model is computationally efficient and provides more accurate thrust estimates than models currently implemented in live experiments, which generally ignore the effects of wind altogether or assume pure axial flow.

Appendix

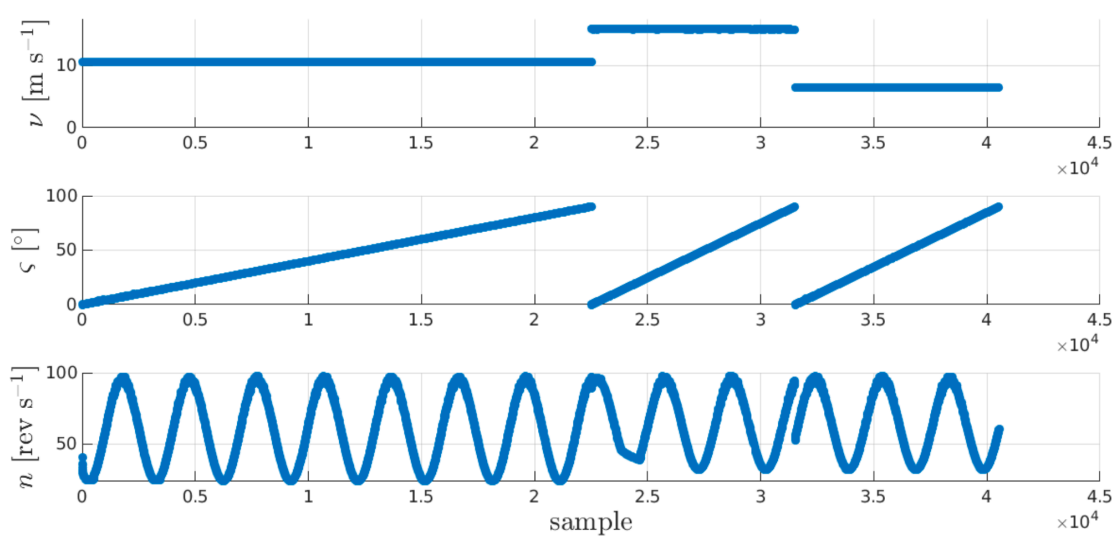

(a) Top: freestream velocity ν, middle: oblique angle ς, and bottom: propeller rotational velocity n.

doi.org/10.32388/WG08LV

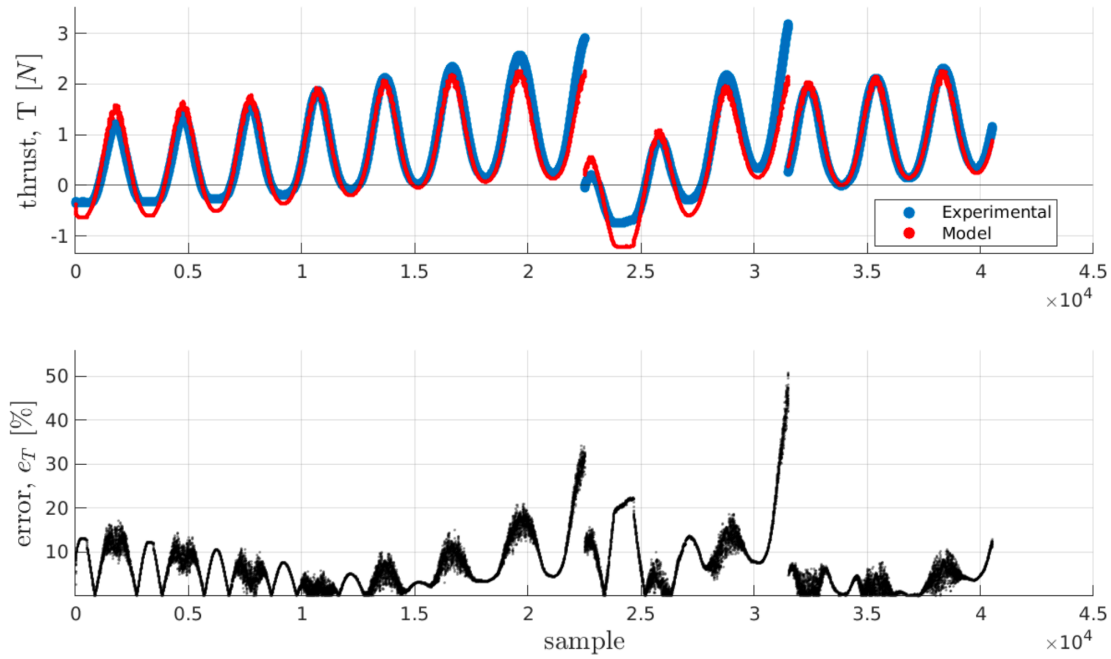

(b) Experimental thrust (top, blue), and modeled thrust (top, red) at every sample. Thrust percent error relative to maximum thrust (bottom).

Figure 10. Oblique flow experiment in wind tunnel conducted by [13] for propeller APC Thin Electric 8x6 (top). Comparison between experimental thrust and modeled thrust (bottom).

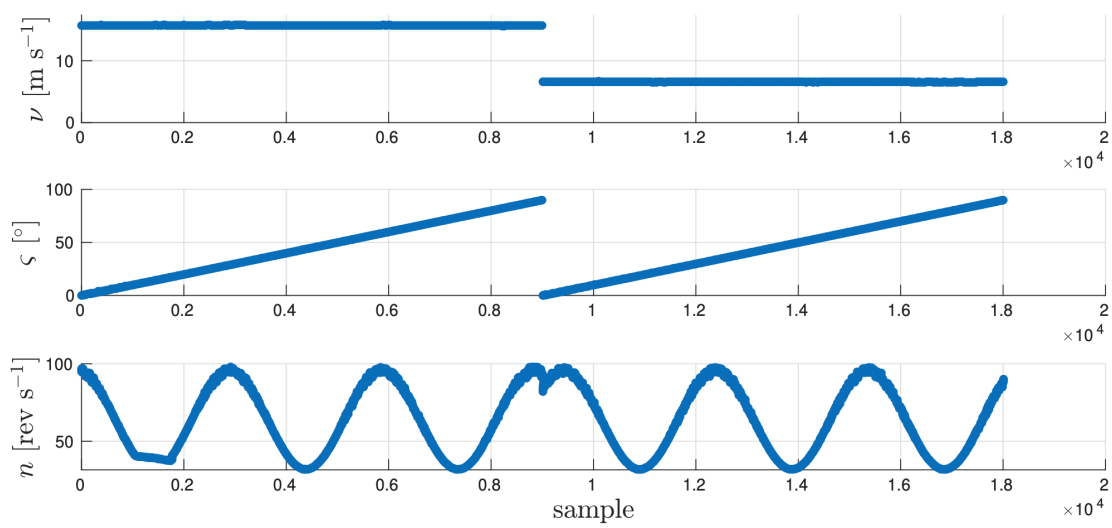

(a) Top: freestream velocity ν, middle: oblique angle ς, and bottom: propeller rotational velocity n.

doi.org/10.32388/WG08LV

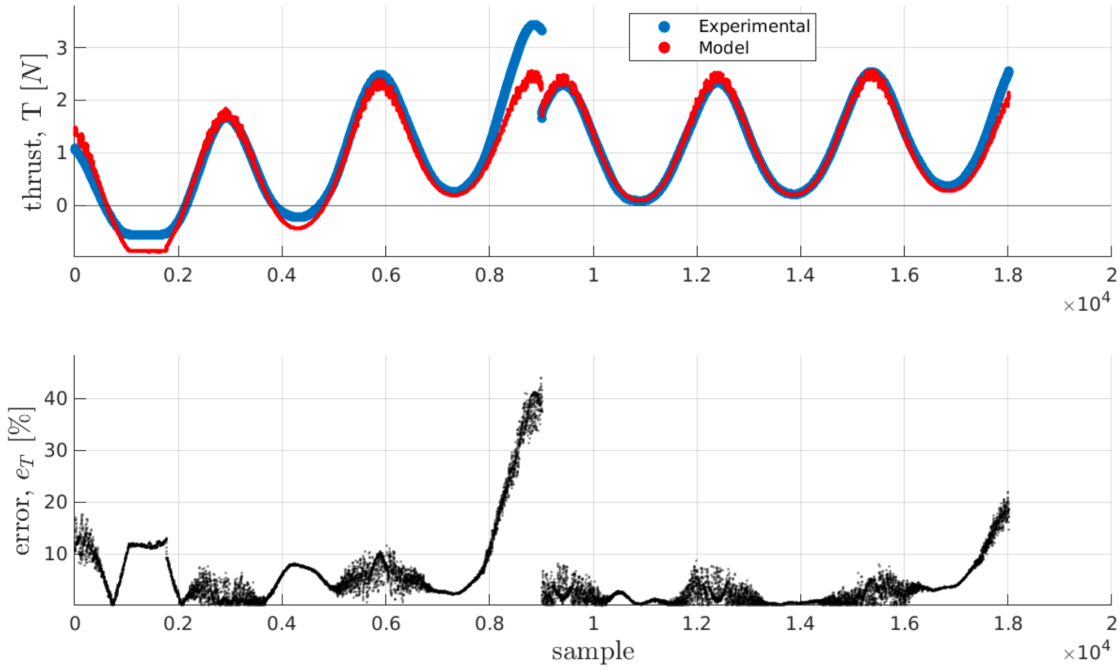

(b) Experimental thrust (top, blue), and modeled thrust (top, red) at every sample. Thrust percent error relative to maximum thrust (bottom).

Figure 11. Oblique flow experiment in wind tunnel conducted by [13] for propeller APC Thin Electric 8x8 (top). Comparison between experimental thrust and modeled thrust (bottom).

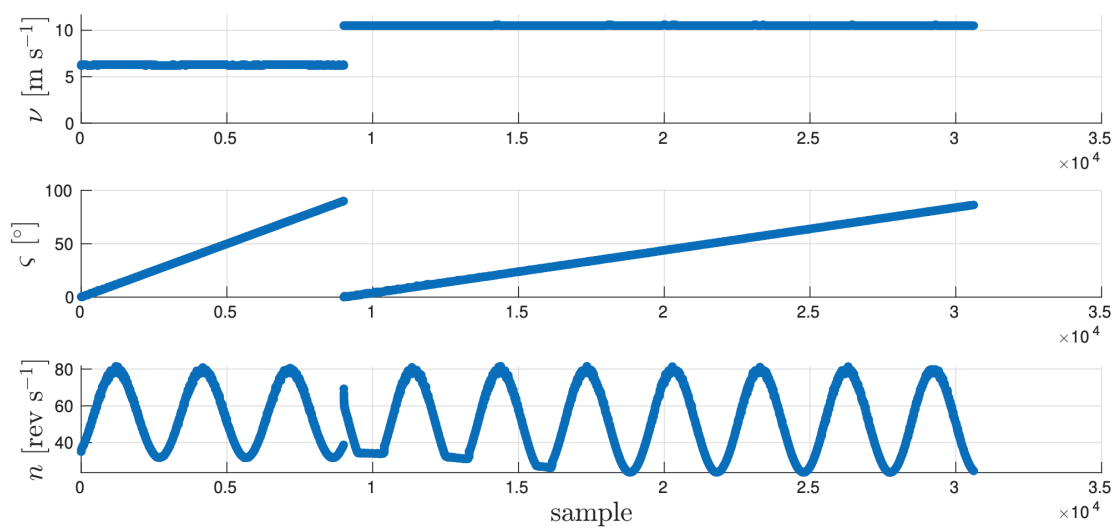

(a) Top: freestream velocity ν, middle: oblique angle ς, and bottom: propeller rotational velocity n.

doi.org/10.32388/WG08LV

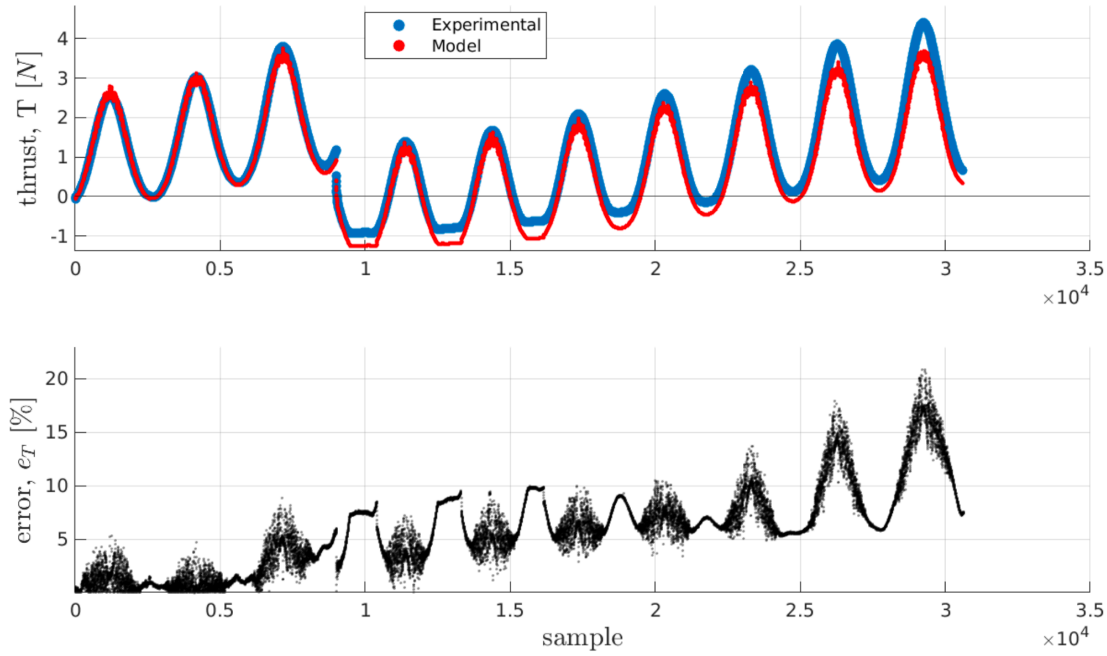

(b) Experimental thrust (top, blue), and modeled thrust (top, red) at every sample. Thrust percent error relative to maximum thrust (bottom).

Figure 12. Oblique flow experiment in wind tunnel conducted by [13] for propeller APC Slow Flyer 10x4.7 (top). Comparison between experimental thrust and modeled thrust (bottom).

Funding Sources

This research was supported by funding from a Natural Sciences and Engineering Research Council of Canada Discovery Grant.

Acknowledgments

We would like to acknowledge Dr. Bart Theys (Katholieke Universiteit Leuven) for providing us their detailed experimental results conducted in a wind tunnel from [12].

References

1. ^*Christopher Silva, Wayne R. Johnson, Eduardo Solis, Michael D. Patterson, Kevin R. Antcliff. (2018). VTOL urban air mobility concept vehicles for technology development. In: AIAA aviation technology, integration, and operations conference.: Atlanta, Georgia. doi:10.2514/6.2018-3847*

2. ^M. Hassanalian, A. Abdelkefi. (2017). Classifications, applications, and design challenges of drones: A review. Progress in Aerospace Sciences. 91:99–131. doi:https://doi.org/10.1016/j.paerosci.2017.04.003
3. ^Eitan Bulka, Meyer Nahon. (2019). Automatic Control for Aerobatic Maneuvering of Agile Fixed-Wing UAVs. Journal of Intelligent and Robotic Systems: Theory and Applications. 93(1-2):85–100. doi:10.1007/s10846-018-0790-z
4. ^https://www.jobyaviation.com/ 2021.
5. a, b, c, d, e, f, g, h, i, jJ. B. Brandt, R. W. Deters, G. K. Ananda, O. D. Dantsker, M. S. Selig. UIUC Propeller Data Site. 2005. Available from: https://m-selig.ae.illinois.edu/props/propDB.html
6. ^H. B. Freeman. (1932). The effect of small angles of yaw and pitch on the characteristics of airplane propellers. University of North Texas Libraries, UNT Digital Library 1932. Report No.: NACA Report No. 389.
7. ^John L. Crigler, Jr. Gilman Jean. (1952). Calculation of aerodynamic forces on a propeller in pitch or yaw. Hampton, VA: University of North Texas Libraries, UNT Digital Library 1952. Report No.: NACA TN-2585.
8. a, b, cJ. Gordon Leishman. (2006). Principles of helicopter aerodynamics. 2nd ed. Cambridge University Press.
9. ^H. Glauert. (1926). A general theory of the autogyro. Cranfield: British Aeronautical Research Committee 1926. Report No.: Reports & Memoranda No. 1111.
10. ^R. T. N. Chen. (1989). A survey of nonuniform inflow models for rotorcraft flight dynamics and control applications. Moffett Field, CA: NASA 1989. Report No.: TM-102219.
11. a, b, c, dWaqas Khan, Meyer Nahon. (2015). A propeller model for general forward flight conditions. International Journal of Intelligent Unmanned Systems. 3(2-3):72–92. doi:10.1108/IJIUS-06-2015-0007
12. a, b, c, d, e, f, g, h, i, jB. Theys, G. Dimitriadis, P. Hendrick, J. De Schutter. (2017). Experimental and numerical study of micro-aerial-vehicle propeller performance in oblique flow. Journal of Aircraft. 54(3):1076–1084. doi:10.2514/1.C033618
13. a, b, c, d, e, f, g, h, i, j, k, lRajan Gill, Raffaello D'Andrea. (2019). Computationally Efficient Force and Moment Models for Propellers in UAV Forward Flight Applications. Drones. 3(4):77. doi:10.3390/drones3040077
14. ^Waqas Khan, Meyer Nahon. (2013). Toward an Accurate Physics-Based UAV Thruster Model. IEEE/ASME Transactions on Mechatronics. 18(4):1269–1279. doi:10.1109/TMECH.2013.2264105

Declarations

Funding: The first author was awarded a McGill University Graduate Excellence Award.

Potential competing interests: No potential competing interests to declare.